ACS OMEGA

Article

Cite This: ACS Omega 2019, 4, 10729−10740

http://pubs.acs.org/journal/acsodf

Oxidative Cleavage of Cellobiose by Lytic Polysaccharide Monooxygenase (LPMO)-Inspired Copper Complexes

Andrea. C. Neira,[†] Paulina R. Martínez-Alanis,[§] Gabriel Aullón,[§] Marcos Flores-Alamo,[‡] Paulino Zerón,[‡] Anna Company,[∥] Juan Chen,[⊥] Johann B. Kasper,[⊥] Wesley R. Browne,[⊥] Ebbe Nordlander,[#] and Ivan Castillo*[,†]

[†]Instituto de Química and [‡]Facultad de Química, División de Estudios de Posgrado, Universidad Nacional Autónoma de México, Circuito Exterior, CU, 04510 Ciudad de México, México

[§]Departament de Química Inorgànica i Orgànica and Institut de Química Teòrica i Computacional, Universitat de Barcelona, Martí i Franquès 1-11, 08028 Barcelona, Spain

[∥]Institut de Química Computacional i Catàlisi (IQCC), Departament de Química, Universitat de Girona, C/ M. Aurèlia Capmany 69, 17003 Girona, Catalonia, Spain

[⊥]Molecular Inorganic Chemistry, Stratingh Institute for Chemistry, Faculty of Science and Health, University of Groningen, Nijenborgh 4, 9747AG Groningen, The Netherlands

[#]Chemical Physics, Department of Chemistry, Lund University, Box 124, SE-221 00 Lund, Sweden

Supporting Information

ABSTRACT: The potentially tridentate ligand bis[(1-methyl-2-benzimidazolyl)ethyl]amine (**2BB**) was employed to prepare copper complexes [(**2BB**)Cu^{I}]OTf and [(**2BB**)-$Cu^{II}(H_2O)_2$]$(OTf)_2$ as bioinspired models of lytic polysaccharide copper-dependent monooxygenase (LPMO) enzymes. Solid-state characterization of [(**2BB**)Cu^{I}]OTf revealed a Cu(I) center with a T-shaped coordination environment and metric parameters in the range of those observed in reduced LPMOs. Solution characterization of [(**2BB**)$Cu^{II}(H_2O)_2$]$(OTf)_2$ indicates that [(**2BB**)-$Cu^{II}(H_2O)_2$]$^{2+}$ is the main species from pH 4 to 7.5; above pH 7.5, the hydroxo-bridged species [{(**2BB**)$Cu^{II}(H_2O)_x$}$_2$(μ-$OH)_2$]$^{2+}$ is also present, on the basis of cyclic voltammetry and mass spectrometry. These observations imply that deprotonation of the central amine of Cu(II)-coordinated **2BB** is precluded, and by extension, amine deprotonation in the histidine brace of LPMOs appears unlikely at neutral pH. The complexes [(**2BB**)Cu^{I}]OTf and [(**2BB**)$Cu^{II}(H_2O)_2$]$(OTf)_2$ act as precursors for the oxidative degradation of cellobiose as a cellulose model substrate. Spectroscopic and reactivity studies indicate that a dicopper(II) side-on peroxide complex generated from [(**2BB**)Cu^{I}]OTf/O_2 or [(**2BB**)$Cu^{II}(H_2O)_2$]$(OTf)_2$/H_2O_2/NEt_3 oxidizes cellobiose both in acetonitrile and aqueous phosphate buffer solutions, as evidenced from product analysis by high-performance liquid chromatography-mass spectrometry. The mixture of [(**2BB**)$Cu^{II}(H_2O)_2$]$(OTf)_2$/H_2O_2/NEt_3 results in more extensive cellobiose degradation. Likewise, the use of both [(**2BB**)Cu^{I}]OTf and [(**2BB**)$Cu^{II}(H_2O)_2$]$(OTf)_2$ with KO_2 afforded cellobiose oxidation products. In all cases, a common Cu(II) complex formulated as [(**2BB**)$Cu^{II}(OH)(H_2O)$]$^{+}$ was detected by mass spectrometry as the final form of the complex.

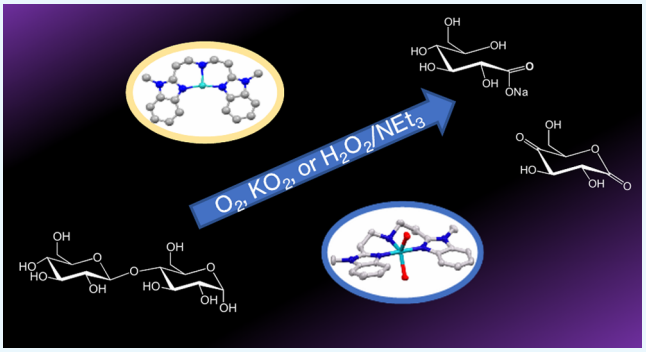

INTRODUCTION

The recently reported lytic polysaccharide monooxygenases (LPMOs),[1] also known as the auxiliary activity (AA) family of copper-dependent enzymes,[2] feature a conserved type 2 copper binding site with a N_3 donor set defined by two imidazoles and a backbone nitrogen from one of the histidine residues, in a structural motif described as the "histidine brace" (Chart 1).[2a,3] These enzymes oxidatively cleave the polymeric chains of recalcitrant polysaccharides to assist hydrolytic enzymes and have potential applications in biomass conversion to renewable biofuels. Recent studies have established some of the aspects that govern substrate binding, such as H-bonding to the primary amine of the histidine brace,[4] as well as the potential involvement of dioxygen[5] or hydrogen peroxide[6] as oxidants. However, details of the mechanism, potential intermediates in the key C−H activation step, and subsequent polysaccharide hydroxylation remain to be determined. Although cupric−superoxo and oxyl complexes have been suggested as the reactive intermediates, a mechanistic insight may be obtained from synthetic models. In this regard, few biomimetic LPMO-

Received: March 21, 2019
Accepted: June 6, 2019
Published: June 20, 2019

Chart 1. (a) Schematic Representation of the Active Site of LPMO, (b) 2BB, and (c) Mercury Diagram of the Dication $[(\mathbf{2BB})Cu^{II}(H_2O)_2]^{2+}$[15]

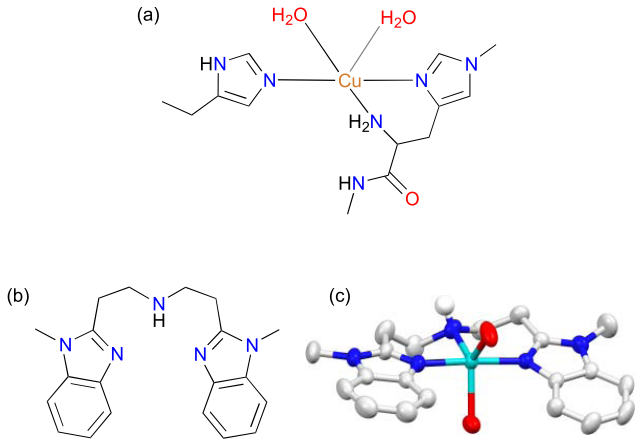

inspired copper complexes have been reported to date,[7] despite the numerous reports on biologically inspired copper–oxygen systems.[8]

Due to the ubiquitous presence of coordinated histidine residues in metalloenzyme active sites, most bioinspired complexes employ amines and nitrogen-containing heterocycles as histidine models. This approach has relied heavily on amine-, pyrazole-, and pyridine-based ligands. In contrast, reports on ligands that incorporate the more electronically relevant imidazolyl and/or benzimidazolyl donor substituents remain relatively scarce,[9] with the notable exception of the binucleating scaffolds developed by the groups of Casella.[10] We have recently exploited 2-substituted benzimidazoles to assemble chelating ligands for mononuclear $Cu^{II/I}$ complexes; these ligands offer versatility as good σ-donors and reasonable π-acceptors toward copper ions, as well as varying degrees of steric protection.[11] Exploration of their reactivity has revealed the formation of free superoxide anions, presumably released by solvent displacement from the putative Cu^{II}-superoxide species obtained from the corresponding cuprous complexes and O_2.[11d] These steps have been suggested to occur in LPMOs on the basis of DFT calculations[5] and recently reported structural data,[6,12] in a rapid inner-sphere reductive activation of O_2.[5]

In this context, we recently reported the use of bis[(1-methyl-2-benzimidazolyl)ethyl]amine (**2BB**,[13,10b] Chart 1) as a simple structural model of the ligand environment in mononuclear active sites of LPMO.[14,15] Our interest was spurred by the presence of a methylated nitrogen atom in one of the histidinic imidazoles of fungal LPMO[2a] and the presence of a central secondary amine available for potential H-bonding with substrates. Additionally, the **2BB**/Cu^{II} system afforded complexes with bonding parameters in the range of those of LPMO active sites (Cu–N distances of ∼1.98 Å, N–Cu–N angles of ∼97 and ∼165°). In continuation of these preliminary studies, we herein report detailed spectroscopic studies of $[(\mathbf{2BB})Cu^{II/I}]^{2+/+}$ complexes, their interaction with O_2, H_2O_2, and KO_2, as well as their oxidative reactivity toward cellobiose as a cellulose model substrate.

RESULTS AND DISCUSSION

Synthesis of Cu^+ Complex. Previous attempts to isolate cuprous **2BB** complexes required for O_2 binding and subsequent reactivity studies were hampered by the low solubility of the tetrafluoroborate or hexafluorophosphate complexes in dichloromethane.[13,14] However, the use of trifluoromethanesulfonate anions (triflate, OTf) resulted in species soluble in acetonitrile amenable for solution characterization and reactivity studies. Electrospray ionization mass spectrometry (ESI-MS) revealed the presence of a peak at m/z 396 assigned to the monomeric $[(\mathbf{2BB})Cu^{I}]^+$ [Figure S1 in the Supporting Information]. Further characterization by ^{1}H NMR and Fourier transform infrared (FTIR) spectroscopy confirmed the identity of $[(\mathbf{2BB})Cu^{I}]OTf$; its ^{1}H NMR spectrum in CD_3CN shows relatively broad aromatic signals for the benzimidazole groups at δ 7.64, 7.24, and 7.06 ppm, the resonance for the *N*-methyl groups was observed at δ 3.42, whereas the methylene protons gave rise to resonances at δ 3.21 ($-CH_2-N$) and 3.01 ppm ($-CH_2-C$). FTIR spectroscopy displayed notable bands at 3273 (w) cm^{-1} assigned to the central amine N–H stretch, 1027 and 1257 (s) assigned to S–O stretching bands of the triflate anion, as well as a pair of strong bands at 1147 and 1227 cm^{-1} assigned to C–F stretching vibrations; a band at 1614 cm^{-1} was assigned to the benzimidazole-based C=N stretching mode. The main differences with the previously reported cupric complex $[(\mathbf{2BB})Cu^{II}(H_2O)_2](OTf)_2$ include the frequencies of the N–H stretch at 3241 (w) cm^{-1}, the slightly higher intensity of the C=N stretching mode previously observed at 1617 cm^{-1}, and the shoulder at 3356 cm^{-1} that was assigned to O–H stretching modes in the cupric complex.

Solid-State Structure of $[(\mathbf{2BB})Cu^{I}]OTf$. $[(\mathbf{2BB})Cu^{I}]OTf$ was dissolved in a minimum amount of anhydrous CH_3CN, and after slow evaporation, colorless X-ray quality crystals of $[(\mathbf{2BB})Cu^{I}]OTf$ were obtained. The metric parameters around the Cu(I) center in the $[(\mathbf{2BB})Cu^{I}]^+$ cation are in the range of those reported for the enzymes, displaying the characteristic T-shape of the reduced form of the active sites of LPMOs, as shown in Figure 1 and Tables S1–S3. The N1–Cu1–N4 open

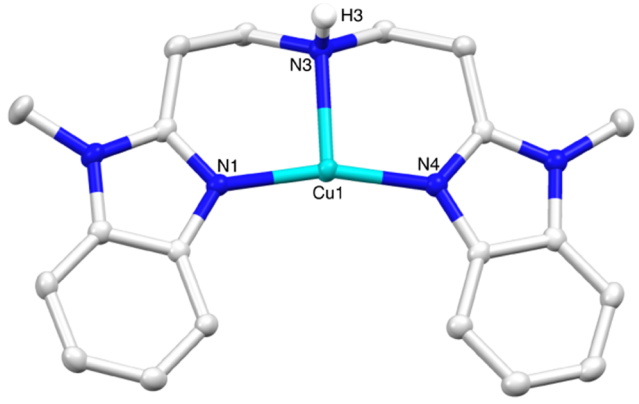

Figure 1. Mercury diagram of $[(\mathbf{2BB})Cu^{I}]^+$ at the 50% probability level. H atoms, except for H3 on the central amine, and the triflate counter ion are omitted for clarity; color code: C, grey; N, blue; Cu, turquoise.

angle of 165° in $[(\mathbf{2BB})Cu^{I}]^+$ is identical to the corresponding one in the AA9–AA11 active sites,[16] whereas the two closed angles, N3–Cu1–N4 and N1–Cu1–N3 of 98.01 and 96.82°, respectively, for $[(\mathbf{2BB})Cu^{I}]^+$, are equivalent to that of 97° in LPMO. A comparison of the bond distances is presented in Table 1, showing a larger Cu–N distance to the central nitrogen donor than that to the benzimidazole N atoms.

DOI: 10.1021/acsomega.9b00785
ACS Omega 2019, 4, 10729–10740

Table 1. Bond Distances and Angles in [(2BB)Cu^{I}]OTf and Comparison with the Corresponding Parameters in Reduced LsAA9A[16]

parameter	[(2BB)Cu]OTf	parameter	Cu(I)LsAA9A
Cu1−N4	1.901 Å	Cu−Nσ (His1)	1.9 Å
Cu1−N1	1.908 Å	Cu−Nε (His78)	2.0 Å
Cu1−N3	2.173 Å	Cu−NH_2(His1)	2.2 Å
N4−Cu1−N1	164.54°	Nσ−Cu−Nε	165°
N4−Cu1−N3	98.01°	Nσ−Cu−NH_2	97°
N1−Cu1−N3	96.82°	Nε−Cu−NH_2	97°

Interestingly, the triflate anion interacts with [(**2BB**)Cu^{I}]$^{+}$ via hydrogen bonding with the central amine N−H, defined by an O2···N3 distance of 3.363(3) Å and an O2···H3−N3 angle of 149(2)°.

Solution Studies of [(2BB)Cu^{II}(H_2O)$_2$](OTf)$_2$. Insight into the nature of the cupric complex in an aqueous solution was gained through equilibrium studies to determine its speciation. Potentiometric titration of **2BB** afforded pK_a values of 3.68, 4.86, and 7.84 for the protonated forms of the two benzimidazolic and amine sites, respectively. The values for the benzimidazolic sites are lower (in water at 25 °C) than those of benzimidazole at 5.58,[17a] 1-methylbenzimidazole, 1-ethylbenzimidazole at 4.88, and even 1-methyl-5-chlorobenzimidazole at 3.88.[17b] Subsequently, the stability constant for [(**2BB**)Cu^{II}(H_2O)$_2$]$^{2+}$ was determined at log K = 12.44 after refinement of the potentiometric data with Hyperquad software,[18] considering temperature, volumes, and concentrations of analytes (HNO_3, NaOH, potassium biphthalate, **2BB**, and its cupric complex, see Figure S2). This log K value is high compared to that of Cu(II) with bidentate 2-hydroxymethylbenzimidazole and 1-methyl-2-hydroxymethylbenzimidazole at 9.30 and 9.66, respectively.[17a]

The species distribution was determined with MEDUSA software[19] (ionic strength 0.1 M $NaNO_3$), where the dicationic species [(**2BB**)Cu^{II}]$^{2+}$ clearly predominates in the pH range of 4−8; see Figure 2. One or two molecules of water are likely

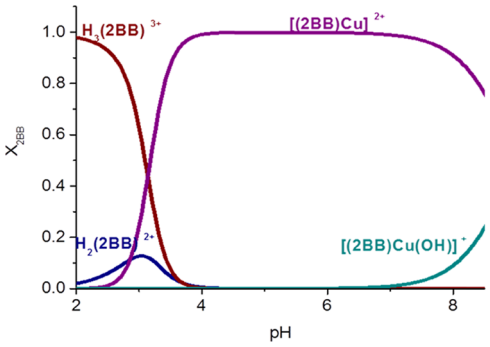

Figure 2. Speciation diagram for [(**2BB**)Cu^{II}]$^{2+}$.

coordinated to the cupric ion in solution to form [(**2BB**)Cu^{II}(H_2O)$_n$]$^{2+}$ (n = 1, 2), as observed in the solid state.[15] Interestingly, a monodeprotonated species is predicted to be present around pH 7.5 and above, which was assigned to a cupric−hydroxo complex [(**2BB**)Cu^{II}(OH)(H_2O)$_{n-1}$]$^{+}$, likely in the form of a bridged dimer [{(**2BB**)Cu^{II}(H_2O)$_{n-1}$}$_2$(μ-OH)$_2$]$^{2+}$, with log K = 15.88. This type of species would be favored over a complex with a deprotonated central amine, on the basis of the additional experimental evidence for a hydroxo-bridged dicopper complex (vide infra). Further support for deprotonation of a coordinated water molecule over an amine donor is provided by studies on the effect of metal coordination on the pK_a values of biologically relevant ligands, with transition-metal ions increasing the acidity by 1−3 log units.[20] These observations suggest that the potential involvement of a deprotonated amine during the catalytic cycle may be ruled out in our system and plausibly in the active site of LPMO as well. In the enzymatic system, the proposed deprotonation of the terminal amine of the histidine brace[12] seems unlikely near neutral pH,[4−6] particularly considering determinations of the pK_a values of terminal amino groups in related ATCUN peptide complexes.[21] Quantum refinement of X-ray and neutron diffraction data also argues against −NH_2 deprotonation.[22]

Electrochemical Studies. The species distribution is supported by electrochemical results obtained at pH 5.0, 7.0, 9.0, and 10.5 of aqueous solutions of [(**2BB**)Cu^{II}(H_2O)$_2$](OTf)$_2$. The system behaves quasireversibly, with one redox wave assigned to the Cu$^{II/I}$ couple at $E_{1/2}$ = 226 mV vs standard hydrogen electrode (SHE) at pH 5.0−7.0, which is in the range of the redox potentials reported for LPMOs (150−370 mV vs SHE). Differences were observed at pH 9.0−10.5; in the former case, a shoulder at a slightly more negative potential indicates the presence of an additional species. This is confirmed at pH 10.5, where the shoulder becomes the only wave observed (Figure 3). In CH_3CN, electrochemical analysis of [(**2BB**)Cu^{I}]OTf shows a quasireversible behavior, with $E_{1/2}$ = 76 mV vs SHE (−272 mV vs ferrocenium/ferrocene, Figure S3).

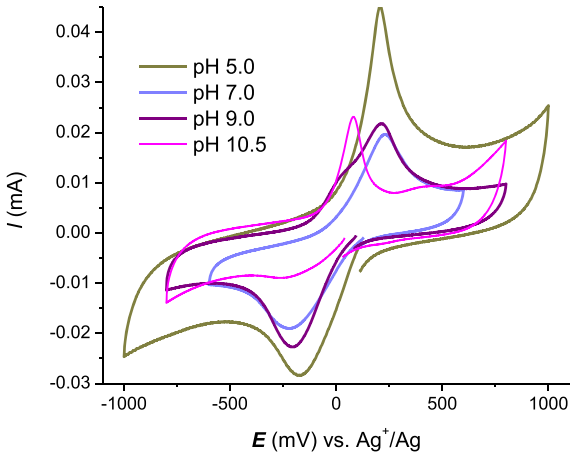

Figure 3. Cyclic voltammograms of 1 mM [(**2BB**)Cu^{II}(H_2O)$_2$](OTf)$_2$ solutions in phosphate buffer (PB) at pH 5.0, 7.0, and 9.0, and in carbonate buffer at pH 10.5, acquired at 1 V s^{-1} with a glassy carbon electrode (at pH 10.5, the system is heterogeneous).

Insight into the identity of the additional species formed at pH 9.0−10.5 was obtained through ESI-MS analysis of a solution of [(**2BB**)Cu^{II}(H_2O)$_2$](OTf)$_2$. A signal was detected at m/z 887, which was assigned to the mixed hydroxo/carbonato-bridged dicopper complex shown in Scheme 1 on the basis of its mass and isotope distribution. The complex detected may be formed upon aerobic CO_2 insertion into an initially formed dihydroxo-bridged dimeric complex [{(**2BB**)Cu^{II}(H_2O)$_x$}$_2$(μ-OH)$_2$]$^{2+}$.[23] UV−vis spectroscopic evidence of the formation of the putative [{(**2BB**)Cu^{II}(H_2O)$_x$}$_2$(μ-OH)$_2$]$^{2+}$ was obtained by addition of NEt_3 to an acetonitrile solution of [(**2BB**)Cu^{II}(H_2O)$_2$](OTf)$_2$ at room temperature.

DOI: 10.1021/acsomega.9b00785
ACS Omega 2019, 4, 10729−10740

Scheme 1. Proposed Hydroxo/Carbonato-Bridged Dicopper Complex Formed from $[(2BB)Cu^{II}(H_2O)_2](OTf)_2$ in Water at pH 9.0 with Experimental (Left) and Simulated Isotopic Mass Spectrometry Patterns (Right)

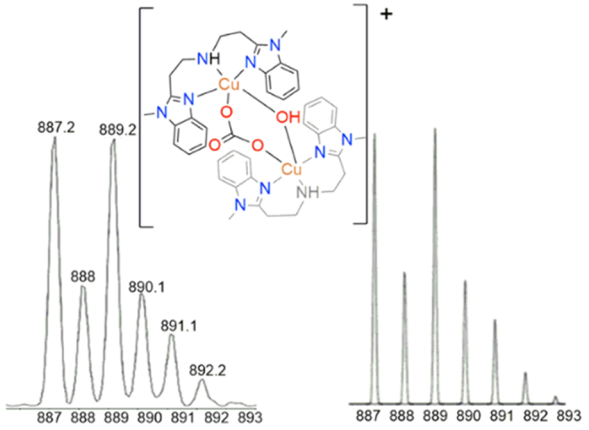

A new band was observed at 330 nm ($\varepsilon \sim 2000\ M^{-1}\ cm^{-1}$), which can be assigned as a hydroxo to Cu(II) ligand-to-metal charge-transfer (LMCT) transition; see Figure S4.

These observations confirm that deprotonation of a coordinated water molecule is more facile than that of the amine in our system. This deprotonation occurs at a higher pH value (7.5) than that used in the study suggesting terminal amine deprotonation (i.e., pH 7.0),[12] further emphasizing that the amine is likely to remain protonated at enzymatic pH. Moreover, the optimum pH value for enzymatic activity is slightly acidic,[4,5] rendering the deprotonation of the terminal amine even less likely.

Reactivity of $[(2BB)Cu^{I}]OTf$ with O_2. The reactivity of $[(2BB)Cu^{I}]OTf$ with dioxygen was explored initially by UV−vis spectroscopy at low temperature in an acetonitrile solution. Gentle bubbling of O_2 through 0.3 mM solutions of $[(2BB)Cu^{I}]OTf$ at 243 K resulted in the appearance of a broad band at 360 nm, assigned to ligand-to-metal charge transfer (LMCT) of a copper−oxygen species, accompanied by d−d transition at 680 nm; a similar behavior was observed in acetone at 193 K. The species was stable for at least an hour, although decay was observed when the temperature was raised; see Figure S5. These changes were not observed under similar conditions or at lower temperature in tetrahydrofuran (THF) solutions, and reactivity studies in this solvent were not pursued. In aqueous phosphate buffer (PB) at 273 K, no significant changes were observed by UV−vis spectroscopy upon bubbling O_2 through in situ-reduced (with 1.2−1.5 equiv of sodium ascorbate) $[(2BB)Cu^{II}(H_2O)_2](OTf)_2$. In both acetonitrile and PB solutions, the products generated at low temperature were characterized by ESI-MS, revealing the presence of an intense signal at m/z 396 assigned to $[(2BB)Cu^{I}]^+$; see Figure S1.

The mixture was characterized by electron paramagnetic resonance (EPR) spectroscopy, revealing that although $[(2BB)Cu^{I}]OTf$ reacts slowly with dioxygen in acetonitrile at 243 K, a signal characteristic of a cupric complex in an axial coordination environment appears after ca. 10 min [$g_{\|}$ = 2.250,

Scheme 2. Proposed Reaction Manifolds and Putative Copper Complexes Generated from $[(2BB)Cu^{I}]^+/O_2$ (Top Left) or $[(2BB)Cu^{II}(S)_2]^{2+}/H_2O_2/NEt_3$ (Top Right)

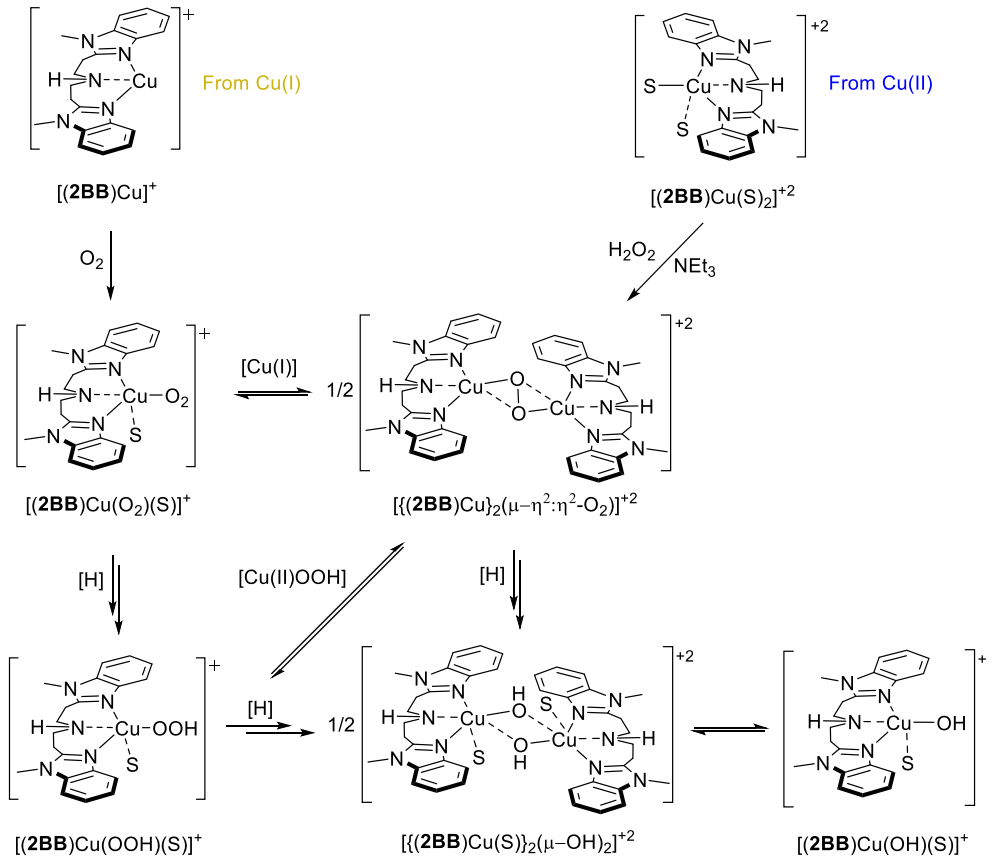

DOI: 10.1021/acsomega.9b00785
ACS Omega 2019, 4, 10729−10740

$g_\perp$ = 2.082, $A_\parallel$ = 423 MHz (151 G), integration 21% relative to Cu(II) external standard]. A reasonable explanation would imply initial formation of an EPR silent cupric−superoxo complex $[(\mathbf{2BB})Cu^{II}(O_2)]^+$, likely in equilibrium with a side-on peroxo-bridged dicopper(II) complex $[\{(\mathbf{2BB})Cu^{II}\}_2(\mu\text{-}\eta^2\text{:}\eta^2\text{-}O_2)]^{2+}$ (on the basis of UV−vis spectroscopy and H_2O_2 reactivity section below). H-abstraction from solvent or cellobiose may result in the EPR-active cupric hydroperoxo $[(\mathbf{2BB})Cu^{II}(OOH)(S)]^+$ and/or the further downstream hydroxo complex $[(\mathbf{2BB})Cu^{II}(OH)(S)]^+$ (S = H_2O, CH_3CN). These species may give rise to the shoulder at 330 nm by UV−vis absorption spectroscopy (Figure S5). Cu(I) oxygenation leading to a Cu(II)-hydroperoxo complex through H-abstraction has been previously observed.[24] Finally, both Cu(II)-hydroperoxo and dicopper(II)-peroxo may further react to generate the final product $[(\mathbf{2BB})Cu^{II}(OH)(S)]^+$, in equilibrium with the dimeric form $[\{(\mathbf{2BB})Cu^{II}(S)_x\}_2(\mu\text{-}OH)_2]^{2+}$ (Scheme 2).

In PB/glycerol at pH 7.0 and 273 K, $[(\mathbf{2BB})Cu^{II}(H_2O)_2](OTf)_2$ reduced in situ with 1.2 equiv of sodium ascorbate produced no changes after bubbling of O_2, changes were not observed. However, addition of cellobiose to the oxygenated PB solution resulted in an axial signal with $g_\parallel$ = 2.275 and $g_\perp$ = 2.054 and $A_\parallel$ = 502 MHz (179 G) and $A_\perp$ = 70 MHz (25 G); see Figure 4; the spectrum was simulated as containing one or

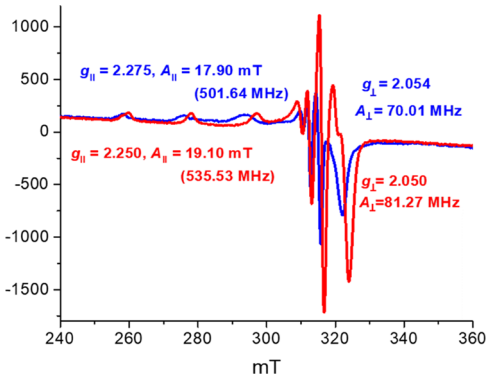

Figure 4. EPR spectra of in situ-generated $[(\mathbf{2BB})Cu^{I}]^+$ with 1.5 equiv of sodium ascorbate after bubbling O_2 and adding 10 equiv of cellobiose (3 mM in PB, blue trace), and mixture of $[(\mathbf{2BB})Cu^{I}]OTf$, 1.2 equiv of KO_2, and 10 equiv of cellobiose (3 mM in CH_3CN, red trace).

two Cu(II) species, with only the former case resulting in a good fit. Examples of mononuclear copper−hydroperoxo complexes featuring tripodal pyridylamine and pyridylamine−thioether ligands have been characterized by EPR spectroscopy and assigned to trigonal bipyramidal [$g_\parallel$ = 2.004, $g_\perp$ = 2.207, $A_\parallel$ = MHz 305 (109 G), $A_\perp$ = 210 MHz (75 G)][25] or square pyramidal geometries [$g_\parallel$ = 2.24, $g_\perp$ = 2.06, $A_\parallel$ = 471 MHz (168 G); $g_\parallel$ = 2.25, $g_\perp$ = 2.04, $A_\parallel$ = 504 MHz (180 G)].[26] A similar situation has been observed with monomeric cupric−hydroxo complexes: EPR spectroscopic data for tripodal complexes have been observed to give rise to "inverse" signals, whereas axial signals with some degree of rhombicity have been observed in the few cases of tetragonal Cu(II)−OH complexes [g_x = 2.032, g_y = 2.055, g_z = 2.185, A_{Cu} = 588 MHz (189 G), A_N = 40−53 MHz (14−19 G)].[27] Resemblance of the parameters to those of the tetragonal species suggests a square pyramidal coordination environment for the putative Cu(II)−hydroperoxo[7c,26] or hydroxo complexes, likely with weak donors in the axial positions $[(\mathbf{2BB})Cu^{II}(OOH)(S)]^+$ or $[(\mathbf{2BB})Cu^{II}(OH)(S)]^+$ (S = solvent, see Scheme 2).

Reactivity of $[(\mathbf{2BB})Cu^{I}]OTf$ and $[(\mathbf{2BB})Cu^{II}(H_2O)_2](OTf)_2$ with KO_2. The reactivity of the copper complexes with a one-electron reduced form of dioxygen was explored with KO_2; this may be important to establish the oxidant in LPMOs, since H_2O_2 has been suggested instead of the originally proposed O_2.[6] Thus, addition of KO_2 to solutions of $[(\mathbf{2BB})Cu^{I}]OTf$ was monitored by UV−vis absorption spectroscopy to identify potential copper−oxygen species, both in acetonitrile and PB solution at pH 7.0. In acetonitrile, the main spectral change consisted of a shoulder at 365 nm, which intensified slightly after addition of cellobiose. Analysis of the reaction mixture by ESI-MS revealed the presence of a peak at m/z 431 assigned to $[(\mathbf{2BB})Cu^{II}(OH)(H_2O)]^+$, along with peaks at m/z 396 and 545 characteristic of $[(\mathbf{2BB})Cu^{I}]^+$ and $[(\mathbf{2BB})Cu^{II}(OTf)]^+$ (Figure S6). When cellobiose was added, ESI-MS evidenced the presence of oxidative degradation products (vide infra). An analogous behavior was observed in PB by UV−vis, although the shoulder was observed at 345 nm. Three relevant peaks were detected by ESI-MS: the one at m/z 412 is consistent with a monooxygenation product $[(\mathbf{2BB})Cu^{II}(O)]^+$, which could correspond to ligand hydroxylation, although such a product was not detected after demetallation with excess aqueous ammonia; a cupryl species cannot be firmly supported without further evidence. A peak at m/z 428 was assigned to the putative cupric−superoxo $[(\mathbf{2BB})Cu^{II}(O_2)]^+$ and the one at m/z 602 was tentatively assigned to $[(\mathbf{2BB})Cu^{II}(O)(OTf)(CH_3CN)]^+$ (Figure S7); the aforementioned species at m/z 396 and 545 were also detected. These observations imply that highly reactive copper−oxygen species are formed in the Cu(I)/KO_2 system, allowing detection of the relatively stable downstream product $[(\mathbf{2BB})Cu^{II}(OH)(H_2O)]^+$.

EPR spectra recorded from flash frozen samples over the course of the reaction reveal that after addition of KO_2 to $[(\mathbf{2BB})Cu^{I}]OTf$ in acetonitrile, a signal characteristic of a cupric complex in an axial environment appears, with $g_\parallel$ = 2.250 and $g_\perp$ = 2.050 and $A_\parallel$ = 536 MHz (191 G) and $A_\perp$ = 81 MHz (29 G), Figure 4. The signal becomes more intense upon addition of cellobiose, possibly due to generation of the proposed $[(\mathbf{2BB})Cu^{II}(OH)(H_2O)]^+$ after H-abstraction,[27] which was detected by ESI-MS. The analogous reaction of $[(\mathbf{2BB})Cu^{II}(H_2O)_2](OTf)_2$ in either CH_3CN or PB solutions with KO_2 did not show considerable changes in its UV−vis absorption spectra, even after addition of cellobiose. No evidence for copper−oxygen species was obtained by ESI-MS or EPR spectroscopy in the reactions of the Cu(II) complex with KO_2. Thus, a cupric−superoxo complex cannot be detected under these conditions.

Reactivity of $[(\mathbf{2BB})Cu]OTf$ and $[(\mathbf{2BB})Cu^{II}(H_2O)_2](OTf)_2$ with H_2O_2. The reaction of $[(\mathbf{2BB})Cu^{II}(H_2O)_2](OTf)_2$ with H_2O_2 was monitored by UV−vis spectroscopy to determine whether different species are formed relative to the reaction of the Cu(I) complex with O_2, both in acetonitrile and PB (pH 7.0). In acetonitrile, no changes with respect to the original spectrum were observed, even after addition of cellobiose; an analogous behavior was observed in PB. High-performance liquid chromatography-mass spectrometry (HPLC-MS) analysis indicated that cellobiose did not undergo degradation. In contrast, reaction of $[(\mathbf{2BB})Cu^{II}(H_2O)_2](OTf)_2$ with 1:1 mixtures of H_2O_2/Et_3N in acetonitrile resulted in spectral changes characterized mainly by an absorbance maximum

DOI: 10.1021/acsomega.9b00785
ACS Omega 2019, 4, 10729−10740

around 365 nm (see Figures S8 and S9) and a d−d transition at 670 nm. Another copper complex appears to be present, on the basis of the shoulder observed at ca. 330 nm. A mixture of the proposed dimeric $[\{(\mathbf{2BB})Cu^{II}\}_2(\mu\text{-}\eta^2\text{:}\eta^2\text{-}O_2)]^{2+}$ and monomeric $[(\mathbf{2BB})Cu^{II}(OOH)(S)]^+$ and/or $[(\mathbf{2BB})Cu^{II}(OH)(S)]^+$ complexes (cf. Scheme 2) may be responsible for the optical features described, with ample precedent for μ-η^2:η^2-peroxo dicopper(II) complexes with intense absorption bands around 360 nm.[10,28] The few examples reported of monomeric, tetragonal cupric hydroperoxo, and hydroxo complexes feature LMCT bands that are blue-shifted relative to the dimeric peroxo-bridged species,[25−27] which is consistent with our observations. The similarity with the UV−vis absorption spectrum of the reaction mixture with $[(\mathbf{2BB})Cu^{I}]^+$ and dioxygen (see Figure S10) further suggests the formation of peroxo dicopper(II) species in the reaction of Cu(I) with O_2 described above. $[\{(\mathbf{2BB})Cu^{II}\}_2(\mu\text{-}\eta^2\text{:}\eta^2\text{-}O_2)]^{2+}$ may form by rapid capture of an initially formed cupric−superoxo $[(\mathbf{2BB})Cu^{II}(O_2)]^+$ by a second equivalent of $[(\mathbf{2BB})Cu^{I}]^+$. The reaction of $[(\mathbf{2BB})Cu^{I}]OTf$ with H_2O_2 was also analyzed by UV−vis absorption and EPR techniques, resulting in spectra with poorly defined features.

The presence of dicopper species in acetonitrile solution was confirmed by cryospray ionization mass spectrometry (CSI-MS) under conditions that are similar to those employed for UV−vis absorption spectroscopy. As soon as 3 equiv of H_2O_2/Et_3N were added to $[(\mathbf{2BB})Cu^{II}(H_2O)_2](OTf)_2$ in acetonitrile, the sample was injected at 243 K, identifying $[(\mathbf{2BB})_2Cu_2^{II}(\mu\text{-}CO_3)(OTf)]^+$, $[(\mathbf{2BB})_2Cu_2^{II}(\mu\text{-}O_2)]^{2+}$, and $[(\mathbf{2BB})Cu^{II}(OH)(H_2O)]^+$. Spectral comparison with the injected sample acquired at 293 K (once the band at 365 nm decayed) shows that similar species are formed, but the bimetallic species are favored at higher temperature, on the basis of their intensities (Table S4 and Figure S11).

Analysis of the reaction mixture by EPR spectroscopy reveals that after reaction of $[(\mathbf{2BB})Cu^{II}(H_2O)_2](OTf)_2$ with 1:1 H_2O_2/Et_3N in acetonitrile, the signal characteristic of a cupric complex in an axial coordination environment becomes weak after ca. 10 min, likely due to formation of the antiferromagnetically coupled $[\{(\mathbf{2BB})Cu^{II}\}_2(\mu\text{-}\eta^2\text{:}\eta^2\text{-}O_2)]^{2+}$; this species is stable for at least 2 h at 243 K, on the basis of UV−vis and EPR measurements.

Addition of the potentially chelating acetate anion (OAc^-, 3 equiv in methanol/acetonitrile) to 0.3 mM $[(\mathbf{2BB})Cu^{II}(H_2O)_2](OTf)_2$ in acetonitrile was tested to interrogate the nature of the dimeric species formed upon addition of 30 equiv of H_2O_2/Et_3N.[29,30] The reaction was monitored by UV−vis absorption spectroscopy at 243 K, showing the generation of the band at 365 nm, attributed to $[\{(\mathbf{2BB})Cu^{II}\}_2(\mu\text{-}\eta^2\text{:}\eta^2\text{-}O_2)]^{2+}$, along with new bands at 414 and 440 nm; see Figure 5.

The band at 365 nm decays over a period of 75 min at 243 K, with concomitant increase in the intensity of the bands at 414 and 440 nm; this transformation occurs almost instantaneously by increasing the temperature to 293 K. Similar results were observed upon addition of O_2, KO_2, or H_2O_2 to cuprous and cupric complexes in the presence of OAc^-. CSI-MS analysis of the final products at 243 K revealed the presence of $[(\mathbf{2BB})_2Cu_2^{II}(\mu\text{-}\eta^2\text{-}OAc)_2(OTf)]^+$ and $[\{(\mathbf{2BB})Cu^{II}\}_2(\mu\text{-}\eta^2\text{:}\eta^2\text{-}O_2)]^{2+}$ (Table S5), with their intensities increasing upon warming up the mixture to 293 K; see Figure S12. EPR spectroscopy reveals that once H_2O_2/Et_3N is added, the signal characteristic of the cupric complex in an axial coordination environment becomes weak after ca. 10 min due to formation of the antiferromagnetically coupled $[\{(\mathbf{2BB})Cu^{II}\}_2(\mu\text{-}\eta^2\text{:}\eta^2\text{-}O_2)]^{2+}$ (Figure S13).

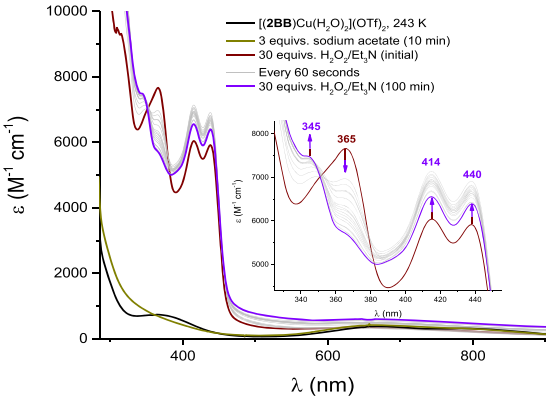

Figure 5. UV−vis absorption spectrum of $[(\mathbf{2BB})Cu^{II}(H_2O)_2](OTf)_2$ (0.3 mM in CH_3CN, 3 equiv of NaOAc in 60 μL of CH_3CN/MeOH, black trace) after addition of 3 equiv of 1:1 H_2O_2/Et_3N (green), and 30 equiv of the same (brown); follow-up of the reaction and the final spectrum after 100 min (purple trace).

Resonance Raman Spectroscopy. Further characterization of the proposed dimer $[\{(\mathbf{2BB})Cu^{II}\}_2(\mu\text{-}\eta^2\text{:}\eta^2\text{-}O_2)]^{2+}$ and the associated complex formed upon addition of NaOAc was attempted by resonance Raman spectroscopy. Since these species give rise to the bands observed by UV−vis absorption spectroscopy at 365 nm and 414 and 440 nm, respectively, measurements were carried out with mixtures of $[(\mathbf{2BB})Cu^{II}(H_2O)_2](OTf)_2$ and 1:1 H_2O_2/Et_3N, with and without added sodium acetate, and excitation at 355 and 457 nm. Raman spectra recorded with excitation at 355 nm was employed at 243 K to favor detection of $[\{(\mathbf{2BB})Cu^{II}\}_2(\mu\text{-}\eta^2\text{:}\eta^2\text{-}O_2)]^{2+}$, whereas excitation at 457 nm was employed at 293 K to favor detection of the unidentified species that gives absorption maxima at 414 and 440 nm (Figures S14 and S15). Although strong signals are present, no isotope-sensitive bands are clearly discernible ($H_2{}^{16}O_2$ vs $H_2{}^{18}O_2$), as the spectra appear to be dominated by ligand-based vibrations. In the case of $[\{(\mathbf{2BB})Cu^{II}\}_2(\mu\text{-}\eta^2\text{:}\eta^2\text{-}O_2)]^{2+}$, the main absorption band in the UV−vis spectrum is associated to a **2BB**-based transition (see the theoretical section and Figures S21 and S22).

Preparative Scale Oxidations of Cellobiose with [(2BB)Cu]OTf and $[(\mathbf{2BB})Cu(H_2O)_2](OTf)_2$. Oxidations of cellobiose using 0.3 mM acetonitrile solutions of $[(\mathbf{2BB})Cu^{II}(H_2O)_2](OTf)_2$, 10 equiv of H_2O_2/Et_3N, and 10 equiv of cellobiose at 243 K were undertaken (cf. Figure S16 and Table S6). Similarly, a comparative reaction was performed by generating the Cu(I) complex in situ from the reduction of $[(\mathbf{2BB})Cu^{II}(H_2O)_2](OTf)_2$ with 10 equiv of sodium ascorbate and subsequent bubbling of O_2, followed by addition of 10 equiv of cellobiose (Figure S17 and Table S7). As a common product of these reactions, sodium gluconate was detected by HPLC-MS (Scheme 3 and Table 2), demonstrating that the $[(\mathbf{2BB})Cu^{II/I}]^{2+/+}$ system has biomimetic activity for oxidative cellobiose degradation in the presence of the appropriate oxidizing agent. It should be noted that the reaction that employed in situ-generated $[(\mathbf{2BB})Cu^{I}]^+$ in PB with O_2 as oxidant is slightly more selective toward gluconate formation, since it was detected in higher yield by HPLC-MS. In PB with H_2O_2/Et_3N as oxidant, the doubly oxidized glucose in Scheme 3 is the main product (Figure S18). The H_2O_2 reaction shows a greater degree of cellobiose degradation, but more products

DOI: 10.1021/acsomega.9b00785
ACS Omega 2019, 4, 10729−10740

Scheme 3. Cellobiose Degradation by $[(2BB)Cu^{II/I}]^{2+/+}$ and Several Oxidants, with Main Products Detected by HPLC-MS

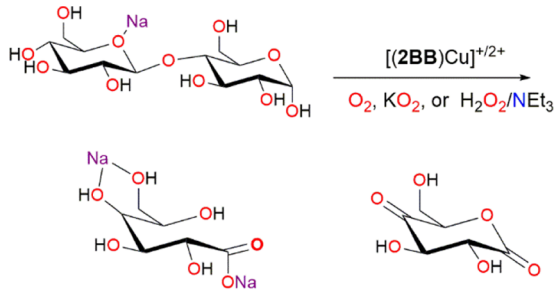

are observed (i.e., H_2O_2 is a more active but less selective oxidant, Figures S16–S18, Tables S6–S8). Reactions were also performed using in situ-reduced cupric complex (with 1.2 and 2.4 equiv ascorbate) and KO_2 as an oxidizing agent, with similar degradation products detected, along with unreacted cellobiose (Table 2). Control experiments with $[(2BB)Cu^{II}(H_2O)_2](OTf)_2$, $CuSO_4$, H_2O_2/NEt_3, and $CuSO_4/H_2O_2/NEt_3$ show no oxidative degradation of cellobiose, although a previously observed dehydration product was detected at m/z 334 in the first case. Care must be exercised in the interpretation of chromatograms, since all samples containing H_2O_2 have a leaching product from the HPLC column (Figure S19).

Glucose oxidation was tested in PB with 0.3 mM $[(2BB)Cu^{II}(H_2O)_2](OTf)_2$ and 10 equiv of H_2O_2/NEt_3 (Figure S20 and Table S9), resulting in mono-oxidation as the major product relative to double oxidation (33 vs 14%). In addition to unreacted glucose, sodium gluconate and glucose aldehyde were detected in small quantities (Table 2). The only precedent of related inorganic systems capable of cleaving glucose derivatives features 4-nitrophenolate as the leaving group.[7b,c]

Computational Studies. The thermodynamic feasibility of the copper–oxygen species that may be formed in the presence of the oxidants tested (O_2, KO_2, and H_2O_2) was evaluated by density functional studies. Reactions of $[(2BB)Cu^{I}]^{+}$, $[(2BB)Cu^{II}]^{2+}$, $[(2BB)Cu^{I}(S)]^{+}$, and $[(2BB)Cu^{II}(S)]^{2+}$ (S = H_2O, CH_3CN) with dioxygen, potassium superoxide, or hydrogen peroxide were evaluated as they appear to generate the dimeric $[\{(2BB)Cu^{II}\}_2(\mu\text{-}\eta^2\text{:}\eta^2\text{-}O_2)]^{2+}$ and potentially $[\{(2BB)Cu^{III}\}_2(\mu\text{-}O)_2]^{2+}$. The optimized structures were validated by comparison of the bonding parameters obtained with those observed for the structurally characterized complexes.

Initial Complexes. $[(2BB)Cu^{I}]^{+}$ and $[(2BB)Cu^{II}]^{2+}$ were considered with either a molecule of water or CH_3CN coordinated, since those solvents were employed for physical measurements and reactivity tests. For both solvents, the coordination of one molecule is energetically favorable, with values between 3 and 30 kcal mol^{-1} (Table 3). The Gibbs free energies for the solvent-coordinated cuprous complexes notwithstanding, calculated for $[(2BB)Cu^{I}(H_2O)]^{+}$ and $[(2BB)Cu^{I}(NCCH_3)]^{+}$ at −3 and −5 kcal mol^{-1}, are rather low compared with the binding constants calculated for their cupric counterparts. This is consistent with the lack of experimental evidence for coordinated solvent molecules in the solid state or in solution by ESI-MS, which can be attributed to the high lability of the Cu(I) centers. The geometries of $[(2BB)Cu^{I}]^{+}$ and the related solvent-coordinated $[(2BB)Cu^{I}(H_2O)]^{+}$ were optimized, and their main geometrical parameters are shown in Table S11. Initial optimization was probed with $[(2BB)Cu^{I}]^{+}$ and subsequently tested with one H_2O ligand, revealing that the nitrogen atoms are maintained in a planar configuration. In the resulting $[(2BB)Cu^{I}(H_2O)]^{+}$, the cuprous center should be defined as four-coordinate but the calculated distance of the nitrogen atom from the central amine to the Cu^{+} ion is considerably longer than in the absence of a bound H_2O (2.407 vs 2.940 Å).

Redox Properties. The redox potentials for $[(2BB)Cu^{II/I}]^{2+/+}$, $[(2BB)Cu(CH_3CN)^{II/I}]^{2+/+}$, and $[(2BB)Cu(H_2O)^{II/I}]^{2+/+}$ couples were estimated by simulating the oxidation process in an acetonitrile solution and referenced to the ferrocenium/ferrocene couple.[31] The calculated potential for trigonal $[(2BB)Cu^{II/I}]^{2+/+}$ was 219 mV, which differs significantly from that calculated with one coordinated molecule of acetonitrile (−135 mV) or water (−305 mV). Since the latter values with solvent coordinated to the copper centers are reasonably close to the experimentally determined data in acetonitrile solution ($E_{1/2}$ = −272 mV), solvent coordination seems to be plausible. In all cases, redox pairs involve a metal-centered process, i.e., the $Cu^{II/I}$ couple.

Dimeric Species. During our attempts to detect copper–oxygen species that may be responsible for the oxidation of cellobiose, the main candidates are the dicopper(II) species $[\{(2BB)Cu^{II}\}_2(\mu\text{-}\eta^2\text{:}\eta^2\text{-}O_2)]^{2+}$ and derivatives having acetate co-ligands. Since several geometries for Cu_2O_2 cores have been described in the literature,[10,28–30] different conformations of the ligands were considered in the molecular optimization of

Table 2. Product Distribution in Cellobiose Degradation Reactions (% Yield by HPLC Integration Relative to Cellobiose)

	assignment			
	cellobiose degradation		glucose degradation	
conditions	O_2 + Cu(I) + 10 equiv sodium ascorbate (H_2O)	H_2O_2/Et_3N + Cu(II) (CH_3CN)	H_2O_2/Et_3N + Cu(II) (PB)	H_2O_2/Et_3N + Cu(II) (PB)
% $[Na + cellobiose]^{+}$	65	8		
% $[Na + cellobiose\text{-}2OH]^{+}$	28	70		
% $[Na + glucose]^{+}$				13
% $[2Na + gluconate]^{+}$	5	3	2	1
X% $[doubly\ oxidized\ glucose + H]^{+}$			18	14
% $[oxidized\ glucose + cellobiose + H]^{+}$			15	33
% $[Na + doubly\ oxidized\ glucose + 2H_2O]^{+}$			37	
% $[Na + glucose\ aldehyde]^{+}$			10	5

DOI: 10.1021/acsomega.9b00785
ACS Omega 2019, 4, 10729–10740

Table 3. Free Energies of Formation of $[(\mathbf{2BB})Cu^{I}(S)]^{+}$ and $[(\mathbf{2BB})Cu^{II}(S)]^{2+}$ with S = H_2O or CH_3CN

reactions	ΔG (gas phase)	ΔG (CH_3CN)
$[(\mathbf{2BB})Cu]^{+} + CH_3CN \rightarrow [(\mathbf{2BB})Cu(CH_3CN)]^{+}$	−11.2	−4.8
$[(\mathbf{2BB})Cu]^{2+} + CH_3CN \rightarrow [(\mathbf{2BB})Cu(CH_3CN)]^{2+}$	−30.9	−16.8
$[(\mathbf{2BB})Cu]^{+} + H_2O \rightarrow [(\mathbf{2BB})Cu(H_2O)]^{+}$	−8.9	−3.1
$[(\mathbf{2BB})Cu]^{2+} + H_2O \rightarrow [(\mathbf{2BB})Cu(H_2O)]^{2+}$	−26.6	−19.0

dicopper species (Figure S21). Their relative energies in acetonitrile were calculated (Table S12) and, as expected, the bimetallic complexes were found to be more stable than the mononuclear T-shape Cu(I) complex by more than 20 kcal mol^{-1} in CH_3CN. Nevertheless, the presence of acetate modifies the dioxygen coordination around the metal centers, predicting the additional species $[\{(\mathbf{2BB})Cu^{II}\}_2(\mu\text{-}\eta^1\text{:}\eta^1\text{-}O_2)(\mu\text{-AcO})]^{+}$.

UV−vis spectra were calculated for complexes with and without acetate as co-ligand (Figure S22). Apparently, coordination of a bridging acetate does not alter the main electronic transitions in the bimetallic complexes. For $[\{(\mathbf{2BB})Cu^{II}\}_2(\mu\text{-}\eta^2\text{:}\eta^2\text{-}O_2)]^{2+}$, an intense band around 330 nm with a **2BB** to dioxygen charge-transfer character was calculated, together with a weaker one at 420 nm having an MLCT character; the first band is consistent with the experimentally observed absorption at 365 nm. For optimized $[\{(\mathbf{2BB})Cu^{II}\}_2(\mu\text{-}\eta^1\text{:}\eta^1\text{-}O_2)(\mu\text{-AcO})]^{+}$ in Figure S21 (species **D**), a medium intensity band is predicted at 420 nm, although the one predicted at around 650 nm is not observed experimentally (Figures S22 and S23); assignment of $[\{(\mathbf{2BB})Cu^{II}\}_2(\mu\text{-}\eta^1\text{:}\eta^1\text{-}O_2)(\mu\text{-AcO})]^{+}$ is only tentative without experimental verification.

CONCLUSIONS

$[(\mathbf{2BB})Cu^{I}]^{+}$ acts as a structural and electronic model of the reduced site of LPMO enzymes. Speciation studies at different pH values, together with electrochemical and mass spectrometry measurements at pH 9.0−10.5, allow us to establish that the pK_a of water molecules bound to **2BB**-coordinated cupric centers is lower than that of the ligand-based amine moiety; this observation is relevant to the enzymatic system, where the proposed deprotonation of the amine of the histidine brace appears to be precluded.

Oxidative cleavage of cellobiose, which was employed as a model polysaccharide substrate, could be effected in the presence of $[(\mathbf{2BB})Cu^{I}]^{+}$ or $[(\mathbf{2BB})Cu^{II}(H_2O)_2]^{2+}$ under appropriate conditions. Clear identification of a copper−oxygen species responsible for the C−H activation that leads to the oxidative cleavage of cellobiose was not possible via low-temperature UV−vis absorption, MS, Raman, or EPR spectroscopic methods in CH_3CN or PB. However, the detection of potential reactive intermediates by ESI-MS, as well as $[(\mathbf{2BB})Cu^{II}(OH)(H_2O)]^{+}$ as the common end product, provides some clues regarding the mechanistic possibilities outlined in Scheme 2.

Moreover, when a more reduced source of the oxidizing agent is provided in our system (i.e., H_2O_2 vs O_2), more degradation of cellobiose was observed by HPLC-MS on a preparative scale, at a cost of lower selectivity. This is consistent with the tentative mechanisms that have been proposed for LPMOs, which imply Cu(I)/H_2O_2 as the most competent combination[32] and H_2O_2 as the natural oxidant for polysaccharide degradation.[6] Nonetheless, identification of the reactive copper−oxygen species involved in the key C−H activations remains a major challenge in copper bioinorganic chemistry.

EXPERIMENTAL SECTION

All synthetic procedures were performed under a dry dinitrogen atmosphere in a glovebox or by conventional Schlenk techniques. THF and diethyl ether were obtained by oxygen- and water-free distilling from sodium benzophenone under a N_2 atmosphere; acetonitrile was distilled from CaH_2. Reagents were purchased from commercial suppliers and used as received; **2BB**[10b,13] and $[(\mathbf{2BB})Cu^{II}(H_2O)_2](OTf)_2$[14,15] were synthesized according to literature procedures. ^1H and ^{13}C NMR spectra were recorded on a JEOL Eclipse 300 or a Bruker Avance DRX spectrometer at 300 and 75 MHz or 500 and 125 MHz, respectively, using the residual protiated solvent signal or TMS as internal references (TMS δ = 0.00, $CHCl_3$ δ = 7.26 ppm). Electrospray ionization mass spectrometry (ESI-MS) experiments were performed with a JEOL JMS-AX505HA spectrometer. Positive-ion FAB$^+$ mass spectra were acquired using a JEOL JMS-SX-102A mass spectrometer operated at an accelerating voltage of 10 kV from a nitrobenzyl alcohol matrix by using xenon atoms at 6 keV. Cryospray ionization mass spectra were recorded on a Bruker MicrOTOF-Q II instrument at Serveis Tècnics of the University of Girona. Samples were introduced into the mass spectrometer ion source by direct infusion using a syringe pump and were externally calibrated using sodium formate. A cryospray attachment was used. Temperature of the nebulizing and drying gases was set at −30 °C. The instrument was operated in both positive- and negative-ion modes.

X-ray Crystallography. A single crystal of $[(\mathbf{2BB})Cu^{I}]$-OTf mounted on a glass fiber was studied with an Oxford Diffraction Gemini "A" diffractometer and a CCD area detector ($\lambda_{MoK\alpha}$ = 0.71073 Å, monochromator: graphite) source equipped with a sealed tube X-ray source at 130 K. Unit cell constants were determined with a set of 15/3 narrow frame/run (1° in ω) scans. A data set consisted of 235 frames of intensity data collected and a crystal-to-detector distance of 55.00 mm. The double pass method of scanning was used to exclude any noise. The collected frames were integrated by using an orientation matrix determined from the narrow frame scans. CrysAlisPro and CrysAlis RED software packages were used for data collection and data integration.[33] Analysis of the integrated data did not reveal any decay. Final cell constants were determined by a global refinement of 12 733 reflections (θ < 29.51°). Collected data were corrected for absorbance by using analytical numeric absorption correction using a multifaceted crystal model based on expressions upon the Laue symmetry using equivalent reflections.[34] Structure solution and refinement were carried out with SHELXS-2014[35a] and SHELXL-2014;[35b] WinGX v2014.1 software[36] was used to prepare material for publication. Full-matrix least-squares refinement was carried out by minimizing $(F_o^2 - F_c^2)^2$. All nonhydrogen atoms were refined anisotropically. The H atom of the amine group (H−N) was located in the difference

DOI: 10.1021/acsomega.9b00785
ACS Omega 2019, 4, 10729−10740

map and refined isotropically with $U_{iso}(H) = 1.2$ for H−N. H atoms attached to C atoms were placed in geometrically idealized positions and refined as riding on their parent atoms, with C−H = 0.95−0.99 Å and with $U_{iso}(H) = 1.2U_{eq}(C)$ for aromatic and methylene groups and $U_{iso}(H) = 1.5U_{eq}(C)$ for methyl groups. A summary of crystallographic data is presented in Tables S1−S3, Supporting Information. Crystallographic data have been deposited at the Cambridge Crystallographic Data Centre CCDC 1821707.

Computational Details. Unrestricted calculations were carried out using the Gaussian 09 package.[37] The hybrid density functional method known as B3LYP was applied.[38] Effective core potentials were used to represent the innermost electrons of the transition-metal atoms and the valence double-ζ quality basis set LANL2DZ associated with the pseudopotentials.[39] The basis set used for the main group elements was 6-31G*.[40] Solvent effects were taken into account through PCM calculations (acetonitrile, ε = 36.64 and water, ε = 78.3553)[41] by using the geometries optimized for the gas phase (single-point calculations). Gibbs free energies in solution were calculated from a thermodynamic cycle of the chemical process by adding solvent effects. Redox potentials were estimated from these solvent calculations by using as reference a value of 5.08 V for the absolute standard hydrogen electrode (SHE) in acetonitrile.[42] The geometrical parameters were analyzed using the SHAPE program.[43]

Vertical excitation energies were obtained from TD-DFT, as implemented in Gaussian 09 in the presence of solvent (acetonitrile). Calculations were performed at the same computational level as singlet states for the dimeric species, using the broken-symmetry approach. Closed-shell singlet and triplet states were also calculated, with small differences.

Electrochemistry. Cyclic voltammetry measurements were made under N_2 in anhydrous CH_3CN, carbonate buffer solution at pH 10.5, or phosphate buffer solutions at pH = 5.0, 7.0, and 9.0, with a CH Instruments potentiostat−galvanostat equipped with a glassy carbon working electrode and a platinum wire auxiliary electrode. Potentials were recorded versus a pseudoreference electrode of AgBr(s)/Ag(wire) immersed in 0.1 M NBu_4Br acetonitrile or distilled water solutions. All voltammograms were started from the current null potential (E_i = 0) and were scanned in both directions, positive and negative, and obtained at scan rates of 0.10 and 0.20 V s^{-1}. In agreement with IUPAC convention, the voltammogram of the ferrocenium-ferrocene (Fc^+/Fc) system[31] was obtained to establish the values of half wave potentials ($E_{1/2}$) from the expression $E_{1/2} = (E_a + E_c)/2$. To obtain the normalized current for each complex, the measured current was divided by the exact molar concentration of the electroactive species.

Solution Studies. For potentiometric titrations, the electrode was calibrated in water, using standard buffers at 25 °C. Commercial 0.1 M NaOH standard solutions were employed, after determination of carbonates present using the Gran Method, ensuring that their concentration was below 5%. The solution of HNO_3 at 8 mM concentration was prepared directly from concentrated acid. Potassium biphthalate was used as an internal standard (oven vacuum-drying 24 h prior to use).

The analytes **2BB** and of $[(\mathbf{2BB})Cu^{II}(H_2O)_2](OTf)_2$ were acidified in a 1:8 ratio with respect to HNO_3 to ensure complete protonation, maintaining in each case a concentration of 1.21×10^{-3} mol L^{-1}. The solutions were maintained in a special cell at 25 °C, stirred under a nitrogen atmosphere, controlling the ionic strength at 0.1 M with $NaNO_3$ under homogeneous conditions. Potentiometric data were obtained in triplicate for acid, base, internal standard, and analytes using a 702SM Titrino automatic titrator and TIAMO1.3 software; for each triplicate, the standard deviation was determined and the final values were averaged. Hyperquad[18] was employed to simulate the data obtained, so that the constants adjusted the model with χ^2 lower than 12.6 with 95% confidence and the species distribution was determined with MEDUSA.[19]

Synthesis of [(2BB)Cu^I]OTf. In an inert atmosphere glovebox, **2BB** (100 mg, 0.30 mmol) and $[Cu^I(NCCH_3)_4]OTf$ (113 mg, 0.30 mmol) were dissolved in 10 mL of anhydrous CH_3CN; after 3 h, volatiles were evaporated under reduced pressure and the solid obtained was washed with 10 mL of anhydrous diethyl ether to afford colorless microcrystalline $[(\mathbf{2BB})Cu^I]OTf$ (39 mg): Yield: 24%; mp 150−152 °C; ^1H NMR (300 MHz, CD_3CN): δ 7.64 (s, 5H, Ar), δ 7.24 (s, 1H, Ar), δ 7.06 (p, J = 7.2 Hz, 5H, Ar), δ 4.97 (dd, J = 13.4, 3.3 Hz, 1H, NH), δ 3.42 (m, 7H, *N*-methyl), δ 3.21 (m, 1H, CH_2N−), δ 3.01 (dt, J = 40.4, 20.2 Hz, 4H, CH_2C−); ESI-MS m/z: $[(\mathbf{2BB})Cu^I]^+$ = 396, $[(\mathbf{2BB})Cu^I(OTf)]^+$ = 545; UV−vis (CH_3CN): 264 (1744), 270 (1577), 282 (7044); IR (KBr): 3273, 2957, 2906, 2852, 1614, 1503, 1481, 1452, 1410, 1327, 1257, 1227, 1147, 1067, 1027, 974, 936, 850, 825, 750, 656, 633, 570, 515, 455, 434; elemental analysis calcd (%) for $C_{21}H_{22}CuF_3N_5O_3S$: C, 46.28; H, 4.07; N, 12.85; found: C, 46.71; H, 4.15; N, 12.75.

Reactivity Studies. The reactivity studies that were carried out with the **2BB**-copper complexes were monitored by UV−vis, ESI-MS, and EPR:

For UV−vis, a 0.3 mM concentration solution of the complex under study was prepared, 2.5 mL was transferred to a 1 cm optical path cell (Schlenk type in the case of cuprous complex, which was sealed with a rubber septum). The cell was transferred to a precooled cryostat and chilled to 243 or 273 K, depending on the solvent used (CH_3CN, PB pH 7.0), with 10 min allowed for equilibration prior to reaction. Oxygenation of the cuprous complex was achieved by gently bubbling dioxygen through the solution using a long needle for 50 s; addition of KO_2, H_2O_2 35%, or H_2O_2/Et_3N dissolved in CH_3CN, H_2O, or a MeOH/CH_3CN mixture (2:3) was performed with 1 equiv of the oxidizing agent in 2 μL of solvent. The stability of the formed species was monitored every 5 min over a period of an hour by measuring the absorbance. Reversibility of each generated system was also determined by bubbling Ar through the solution for 50 s using a long needle. Once the copper−oxygen species was formed, 10 equiv of cellobiose as a substrate was added while stirring in 20 μL of water or a 2:3 H_2O/CH_3CN mixture; the samples were monitored every 5 min over a period of 40 min by measuring the absorbance. The same samples were injected in ESI-MS spectrometers under appropriate conditions.

Characterization by X-band electron spin resonance (EPR) spectroscopy was undertaken in frozen acetonitrile or PB pH 7.0/glycerol. Two hundred microliters of a 3 mM stock solution of the cuprous or cupric complex in CH_3CN or PB/glycerol were placed in quartz EPR tubes ($[(\mathbf{2BB})Cu^I]OTf$ was prepared in a dinitrogen-filled glovebox) and were sealed with rubber septa. Samples were frozen in liquid nitrogen before acquisition at 77 K for CH_3CN and PB/glycerol. The tubes were warmed in ice (273 for PB solution) or ice/acetone (243 K for CH_3CN solution) baths until the samples became

DOI: 10.1021/acsomega.9b00785
ACS Omega 2019, 4, 10729−10740

fluid. Oxygenation of cuprous complexes was achieved by bubbling O_2 through the solutions using a long needle for 50 s. The oxidizing agents used were as follows: KO_2 in 1:1 methanol/acetonitrile or H_2O; H_2O_2, or H_2O_2/Et_3N, maintaining 1 equiv of the oxidizing agent in 2 μL of solution. After addition, spectra were acquired again at 77 or 133 K, respectively. After formation of copper−oxygen species, 10 equiv of cellobiose dissolved in 20 μL of water or a 2:3 $MeOH/CH_3CN$ mixture was added and the spectra were acquired again at 77 K. In situ generation of the Cu(I) complex from $[(\mathbf{2BB})Cu^{II}(H_2O)_2](OTf)_2$ was achieved by adding 1.2 equiv of sodium ascorbate in 20 μL of distilled water or a 2:3 $MeOH/CH_3CN$ mixture.

Raman spectra at 355 and 405 nm were recorded at −30 °C (QNW temperature control cell holder) and room temperature. Raman spectra recorded at 355 (10 mW Cobalt lasers) and 457 (50 mW Cobalt lasers) nm used a home-built system in which the laser was focused on the sample in a 180° backscattering arrangement and Raman scattering was collected, collimated, and subsequently refocused via a pair of 2.5 cm diameter planoconvex lens (f = 15 and 10 cm, respectively). The collected light was filtered by an appropriate long pass edge filter (Semrock) and dispersed by a Shamrock500i spectrograph (slit width 80 μm, Andor Technology) with a 2400 L/mm grating blazed at 300 nm and a Shamrock300i spectrograph (slit width 80 μm, Andor Technology) with a 1200 L/mm grating blazed at 500 nm, respectively. Data were recorded using Andor Solis (Andor Technology) with spectral calibration performed using the Raman spectrum of acetonitrile/toluene 50:50 (v/v).[44] Samples were held in quartz 1 cm path length cuvettes. Spectra analysis and processing was performed using the program Spectragryph 1.2.11.[45]

Preparative Scale Cellobiose and Glucose Degradation. Studies were carried out with 3 mL of **2BB**−Cu complexes and 10 equiv of oxidizing agent or 1 atmosphere of O_2 at 273 K (PB) or 243 K (CH_3CN) and 10 equiv of cellobiose or glucose in 1 mL of distilled water. The mixtures were stirred for 2 h prior to characterization by HPLC-MS with an Agilent 1200 infinity Q-ToF spectrometer equipped with a Poroshell 120 column.

■ ASSOCIATED CONTENT

Supporting Information

The Supporting Information is available free of charge on the ACS Publications website at DOI: 10.1021/acsomega.9b00785.

Materials, spectroscopic data, and methods; electrospray mass spectrum; summary of crystallographic data; bond lengths; cyclic voltammograms; UV−vis spectrum; general procedure for sample preparations in reactivity studies (PDF)

■ AUTHOR INFORMATION

Corresponding Author

*E-mail: joseivan@unam.mx.

ORCID

Gabriel Aullón: 0000-0001-7519-4522
Anna Company: 0000-0003-4845-4418
Wesley R. Browne: 0000-0001-5063-6961
Ivan Castillo: 0000-0002-4876-4339

Author Contributions

The manuscript was written through contributions of all authors. All authors have given approval to the final version of the manuscript.

Notes

The authors declare no competing financial interest.

■ ACKNOWLEDGMENTS

The authors thank Carmen Márquez and Lucero Ríos for mass spectrometry, María de la Paz Orta for combustion analysis, Rocío Patiño for IR, and Virginia Gómez-Vidales for EPR determinations; G.A. and P.R.M.A. acknowledge IQTC-UB for computational resources; AC MINECO Spain CTQ2016-77989-P; A.C.N., E.N., and I.C., the Swedish Research Council (2014-0429); J.C., the Chinese Scholarship Council; J.B.K. and W.R.B., the Netherlands Ministry of Education, Culture and Science (Gravity Program 024.001.035); A.C.N. and I.C., DGAPA-PAPIIT (IN210214 and IN203317), CONACyT (Beca 293842), and CONACyT-ANUIES (ECOS 291247) for financial support.

■ REFERENCES

(1) (a) Phillips, C. M.; Beeson, W. T., IV; Cate, J. H.; Marletta, M. A. Cellobiose Dehydrogenase and a Copper-Dependent Polysaccharide Monooxygenase Potentiate Cellulose Degradation by Neurospora crassa. *ACS Chem. Biol.* **2011**, *6*, 1399. (b) Beeson, W. T.; Phillips, C. M.; Cate, J. H. D.; Marletta, M. A. Oxidative Cleavage of Cellulose by Fungal Copper-Dependent Polysaccharide Monooxygenases. *J. Am. Chem. Soc.* **2012**, *134*, 890.

(2) (a) Quinlan, R. J.; Sweeney, M. D.; Lo Leggio, L.; Otten, H.; Poulsen, J.-C. N.; Johansen, K. S.; Krogh, K. B. R. M.; Jorgensen, C. I.; Tovborg, M.; Anthonsen, A.; Tryfona, T.; Walter, C. P.; Dupree, P.; Xu, F.; Davies, G. J.; Walton, P. H. Insights into the oxidative degradation of cellulose by a copper metalloenzyme that exploits biomass components. *Proc. Natl. Acad. Sci. U.S.A.* **2011**, *108*, 15079. (b) Hemsworth, G. R.; Taylor, E. J.; Kim, R. Q.; Gregory, R. C.; Lewis, S. J.; Turkenburg, J. P.; Parkin, A.; Davies, G. J.; Walton, P. H. The Copper Active Site of CBM33 Polysaccharide Oxygenases. *J. Am. Chem. Soc.* **2013**, *135*, 6069. (c) Hemsworth, G. R.; Henrissat, B.; Davies, G. J.; Walton, P. H. Discovery and characterization of a new family of lytic polysaccharide mono-oxygenases. *Nat. Chem. Biol.* **2014**, *10*, 122.

(3) (a) Lieberman, R. L.; Rosenzweig, A. C. Crystal structure of a membrane-bound metalloenzyme that catalyses the biological oxidation of methane. *Nature* **2005**, *434*, 177. (b) Balasubramanian, R.; Smith, S. M.; Rawat, S.; Yatsunyk, L. A.; Stemmler, T. L.; Rosenzweig, A. C. Oxidation of methane by a biological dicopper centre. *Nature* **2010**, *465*, 115.

(4) Frandsen, K. E. H.; Simmons, T. J.; Dupree, P.; Poulsen, J.-C. N.; Hemsworth, G. R.; Ciano, L.; Johnston, E. M.; Tovborg, M.; Johansen, K. S.; von Freiesleben, P.; Marmuse, L.; Fort, S.; Cottaz, S.; Driguez, H.; Henrissat, B.; Lenfant, N.; Tuna, F.; Baldansuren, A.; Davies, G. J.; Lo Leggio, L.; Walton, P. H. The molecular basis of polysaccharide cleavage by lytic polysaccharide monooxygenases. *Nat. Chem. Biol.* **2016**, *12*, 298.

(5) Kjaergaard, C. H.; Qayyum, M. F.; Wong, S. D.; Xu, F.; Hemsworth, G. R.; Walton, D. J.; Young, N. A.; Davies, G. J.; Walton, P. H.; Johansen, K. S.; Hodgson, K. O.; Hedman, B.; Solomon, E. I. Spectroscopic and computational insight into the activation of O_2 by the mononuclear Cu center in polysaccharide monooxygenases. *Proc. Nat. Acad. Sci. U.S.A.* **2014**, *111*, 8797.

(6) Bissaro, B.; Rohr, A. K.; Muller, G.; Chylenski, P.; Skaugen, M.; Forsberg, Z.; Horn, S. J.; Vaaje-Kolstad, G.; Eijsink, V. G. H. Oxidative cleavage of polysaccharides by monocopper enzymes depends on H_2O_2. *Nat. Chem. Biol.* **2017**, *13*, 1123.

DOI: 10.1021/acsomega.9b00785
ACS Omega 2019, 4, 10729−10740

(7) (a) Neisen, B. D.; Gagnon, N. L.; Dhar, D.; Spaeth, A. D.; Tolman, W. B. Formally Copper(III)−Alkylperoxo Complexes as Models of Possible Intermediates in Monooxygenase Enzymes. *J. Am. Chem. Soc.* **2017**, *139*, 10220. (b) Concia, A. L.; Beccia, M. R.; Orio, M.; Ferre, F. T.; Scarpellini, M.; Biaso, F.; Guigliarelli, B.; Réglier, M.; Simaan, A. J. Copper Complexes as Bioinspired Models for Lytic Polysaccharide Monooxygenases. *Inorg. Chem.* **2017**, *56*, 1023. (c) Muthuramalingam, S.; Maheshwaran, D.; Velusamy, M.; Mayilmurugan, R. Regioselective oxidative carbon-oxygen bond cleavage catalysed by copper(II) complexes: A relevant model study for lytic polysaccharides monooxygenases activity. *J. Catal.* **2019**, *372*, 352.

(8) (a) Itoh, S. Developing Mononuclear Copper−Active-Oxygen Complexes Relevant to Reactive Intermediates of Biological Oxidation Reactions. *Acc. Chem. Res.* **2015**, *48*, 2066. (b) Quist, D. A.; Díaz, D. E.; Liu, J. J.; Karlin, K. D. Activation of dioxygen by copper metalloproteins and insights from model complexes. *J. Biol. Inorg. Chem.* **2017**, *22*, 253.

(9) (a) Thompson, L. K.; Ramaswamy, B. S.; Dawe, R. D. Nickel(II) and copper(II) complexes of the 'tripod' ligand tris(2-benzimidazylmethyl)amine. *Can. J. Chem.* **1978**, *56*, 1311. (b) Addison, A. W.; Hendriks, H. M. J.; Reedijk, J.; Thompson, L. K. Copper complexes of the "tripod" ligand tris(2-benzimidazolylmethyl)amine: five- and six-coordinate copper(II) derivatives and some copper(I) derivatives. *Inorg. Chem.* **1981**, *20*, 103. (c) Balamurugan, R.; Palaniandavar, M.; Gopalan, R. S. Trigonal planar copper(I) complex: synthesis, structure, and spectra of a redox pair of novel copper(II/I) complexes of tridentate bis(benzimidazol-2′-yl) ligand framework as models for electron-transfer copper proteins. *Inorg. Chem.* **2001**, *40*, 2246. (d) Vaidyanathan, M.; Balamurugan, R.; Sivagnanam, U.; Palaniandavar, M. Synthesis, structure, spectra and redox of Cu(II) complexes of chelating bis(benzimidazole)—thioether ligands as models for electron transfer blue copper proteins. *J. Chem. Soc., Dalton Trans.* **2001**, 3498. (e) Seo, M. S.; Kim, N. H.; Cho, K.-B.; So, J. E.; Park, S. K.; Clémancey, M.; Garcia-Serres, R.; Latour, J. -M; Shaik, S.; Nam, W. A mononuclear nonheme iron(IV)-oxo complex which is more reactive than cytochrome P450 model compound I. *Chem. Sci.* **2011**, *2*, 1039.

(10) (a) Casella, L.; Gullotti, M.; Radaelli, R.; Di Gennaro, P. A tyrosinase model system. Phenol ortho-hydroxylation by a binuclear three-coordinate copper(I) complex and dioxygen. *J. Chem. Soc., Chem. Commun.* **1991**, 1611. (b) Casella, L.; Monzani, E.; Gullotti, M.; Gliubich, F.; De Gioia, L. Cytochrome c oxidase models: synthesis and reactivity of iron(III)−copper(II) complexes of deuterohaemin−polybenzimidazole dinucleating ligands. *J. Chem. Soc., Dalton Trans.* **1994**, 3203. (c) Casella, L.; Monzani, E.; Gullotti, M.; Cavagnino, D.; Cerina, G.; Santagostini, L.; Ugo, R. Functional Modeling of Tyrosinase. Mechanism of Phenol ortho-Hydroxylation by Dinuclear Copper Complexes. *Inorg. Chem.* **1996**, *35*, 7516. (d) Garcia-Bosch, I.; Company, A.; Frisch, J. R.; Torrent-Sucarrat, M.; Cardellach, M.; Gamba, I.; Güell, M.; Casella, L.; Que, L., Jr.; Ribas, X.; Luis, J. M.; Costas, M. O_2 Activation and Selective Phenolate ortho Hydroxylation by an Unsymmetric Dicopper μ-η1:η1-Peroxido Complex. *Angew. Chem., Int. Ed.* **2010**, *49*, 2406.

(11) (a) Rodríguez Solano, L. A.; Aguiñiga, I.; López-Ortíz, M.; Tiburcio, R.; Luviano, A.; Regla, I.; Santiago-Osorio, E.; Ugalde-Saldívar, V. M.; Toscano, R. A.; Castillo, I. Bis(2-methylbenzimidazolyl)amine-Derived Copper Complexes and Their Antineoplastic Activity. *Eur. J. Inorg. Chem.* **2011**, 3454. (b) Castillo, I.; Ugalde-Saldívar, V. M.; Rodríguez Solano, L. A.; Sánchez Eguía, B. N.; Zeglio, E.; Nordlander, E. Structural, spectroscopic, and electrochemical properties of tri- and tetradentate N_3 and N_3S copper complexes with mixed benzimidazole/thioether donors. *Dalton Trans.* **2012**, *41*, 9394. (c) Martínez-Alanis, P. R.; Sánchez-Eguía, B. N.; Ugalde-Saldívar, V. M.; Regla, I.; Demare, P.; Aullón, G.; Castillo, I. Copper Versus Thioether-Centered Oxidation: Mechanistic Insights into the Non-Innocent Redox Behavior of Tripodal Benzimidazolylaminothioether Ligands. *Chem. - Eur. J.* **2013**, *19*, 6067. (d) Sánchez-Eguía, B. N.; Flores-Alamo, M.; Orio, M.; Castillo, I. Side-on cupric−superoxo triplet complexes as competent agents for H-abstraction relevant to the active site of PHM. *Chem. Commun.* **2015**, *51*, 11134.

(12) Bacik, J.-P.; Mekasha, S.; Forsberg, Z.; Kovalevsky, A. Y.; Vaaje-Kolstad, G.; Eijsink, V. G. H.; Nix, J. C.; Coates, L.; Cuneo, M. J.; Unkefer, C. J.; Chen, J. C. Neutron and Atomic Resolution X-ray Structures of a Lytic Polysaccharide Monooxygenase Reveal Copper-Mediated Dioxygen Binding and Evidence for N-Terminal Deprotonation. *Biochemistry* **2017**, *56*, 2529.

(13) Sorrell, T. N.; Vankai, V. A.; Garrity, M. L. Synthesis and reactivity of dinuclear copper complexes having a m-xylyl spacer between coordination units. *Inorg. Chem.* **1991**, *30*, 207.

(14) Casella, L.; Carugo, O.; Gullotti, M.; Doldi, S.; Frassoni, M. Synthesis, Structure, and Reactivity of model complexes of copper nitrite reductase. *Inorg. Chem.* **1996**, *35*, 1101.

(15) Castillo, I.; Neira, A. C.; Nordlander, E.; Zeglio, E. Bis(benzimidazolyl)amine copper complexes with a synthetic 'histidine brace' structural motif relevant to polysaccharide monooxygenases. *Inorg. Chim. Acta.* **2014**, *422*, 152.

(16) Frandsen, K. E. H.; Poulsen, J.-C. N.; Tandrup, T.; Lo Leggio, L. Unliganded and substrate bound structures of the cellooligosaccharide active lytic polysaccharide monooxygenase LsAA9A at low pH. *Carbohydrate Res.* **2017**, *448*, 187.

(17) (a) Lane, T. J.; Quinlan, R. Metal binding of the benzimidazoles. *J. Am. Chem. Soc.* **1960**, *82*, 2994. (b) Davies, M. T.; Mamalis, P.; Petrow, V.; Sturgeon, B. J. The preparation and spectrographic properties of some benziminazole-cobalt coordination compounds. *J. Pharm. Pharmacol.* **1951**, *3*, 420.

(18) Gans, P.; Sabatini, A.; Vacca, A. Investigation of equilibria in solution. Determination of equilibrium constants with the HYPERQUAD suite of programs. *Talanta* **1996**, *43*, 1739.

(19) Puigdomenech, I. *MEDUSA: Make Equilibrium Diagrams Using Sophisticated Algorithms*; KTH, Stockholm, 2009.

(20) Martin, R. B. Pyrrole hydrogen ionization of imidazole derivatives in metal ion complexes and carbonic anhydrase. *Proc. Nat. Acad. Sci. U.S.A.* **1974**, *71*, 4346.

(21) (a) Miyamoto, T.; Kamino, S.; Odani, A.; Hiromura, M.; Enomoto, S. Basicity of N-Terminal amine in ATCUN peptide regulates stability constant of albumin-like Cu^{2+} complex. *Chem. Lett.* **2013**, *42*, 1099. (b) Kandemir, B.; Kubie, L.; Guo, Y.; Sheldon, B.; Bren, K. L. Hydrogen evolution from water under aerobic conditions catalyzed by a cobalt ATCUN Metallopeptide. *Inorg. Chem.* **2016**, *55*, 1355.

(22) Caldararu, O.; Oksanen, E.; Ryde, U.; Hedegard, E. D. Mechanism of hydrogen peroxide formation by lytic polysaccharide monooxygenase. *Chem. Sci.* **2019**, *10*, 576.

(23) (a) Mukherjee, J.; Balamurugan, V.; Hundal, M. S.; Mukherjee, R. Fixation of CO_2 in air: synthesis and crystal structure of a μ_3-CO_3-bridged tricopper(II) compound. *J. Chem. Sci.* **2005**, *117*, 111. (b) Das, B.; Bhadbhade, M.; Thapper, A.; Ling, C. D.; Colbran, S. B. A new tri-nuclear Cu-carbonate cluster utilizing CO_2 as a C1-building block − reactive intermediates, a probable mechanism, and EPR and magnetic studies. *Dalton Trans.* **2019**, *48*, 3576.

(24) Fujii, T.; Yamaguchi, S.; Funahashi, Y.; Ozawa, T.; Tosha, T.; Kitagawa, T.; Masuda, H. Mononuclear copper(II)−hydroperoxo complex derived from reaction of copper(I) complex with dioxygen as a model of DβM and PHM. *Chem. Commun.* **2006**, 4428.

(25) Wada, A.; Harata, M.; Hasegawa, K.; Jitsukawa, K.; Masuda, H.; Mukai, M.; Kitagawa, T.; Einaga, H. Structural and Spectroscopic Characterization of a Mononuclear Hydroperoxo-Copper(II) Complex with Tripodal Pyridylamine Ligands. *Angew. Chem., Int. Ed.* **1998**, *37*, 798.

(26) (a) Kodera, M.; Kita, T.; Miura, I.; Nakayama, N.; Kawata, T.; Kano, K.; Hirota, S. Hydroperoxo−Copper(II) Complex Stabilized by N_3S-Type Ligand Having a Phenyl Thioether. *J. Am. Chem. Soc.* **2001**, *123*, 7715. (b) Maiti, D.; Lucas, H. R.; Narducci Sarjeant, A. A.; Karlin, K. D. Aryl Hydroxylation from a Mononuclear Copper-Hydroperoxo Species. *J. Am. Chem. Soc.* **2007**, *129*, 6998.

(27) Donoghue, P. J.; Tehranchi, J.; Cramer, C. J.; Sarangi, R.; Solomon, E. I.; Tolman, W. B. Rapid C−H Bond Activation by a

DOI: 10.1021/acsomega.9b00785
ACS Omega 2019, 4, 10729−10740

Monocopper(III)−Hydroxide Complex. *J. Am. Chem. Soc.* **2011**, *133*, 17602.
(28) (a) Baldwin, M. J.; Root, D. E.; Pate, J. E.; Fujisawa, K.; Kitajima, N.; Solomon, E. I. Spectroscopic studies of side-on peroxide-bridged binuclear copper(II) model complexes of relevance to oxyhemocyanin and oxytyrosinase. *J. Am. Chem. Soc.* **1992**, *114*, 10421. (b) Pidcock, E.; Obias, H. V.; Abe, M.; Liang, H.-C.; Karlin, K. D.; Solomon, E. I. Spectroscopic and Theoretical Studies of Oxygenated Dicopper(I) Complexes Containing Hydrocarbon-Linked Bis[2-(2-pyridyl)ethyl]amine Units: Investigation of a Butterfly $[Cu_2(\mu\text{-}\eta^2\text{:}\eta^2)(O_2)]^{2+}$ Core. *J. Am. Chem. Soc.* **1999**, *121*, 1299.
(29) Ottenwaelder, X.; Rudd, D. J.; Corbett, M. C.; Hodgson, K. O.; Hedman, B.; Stack, T. D. P. Reversible O−O bond cleavage in copper-dioxygen isomers: impact of anion basicity. *J. Am. Chem. Soc.* **2006**, *128*, 9268.
(30) Funahashi, Y.; Nishikawa, T.; Wasada-Tsutsui, Y.; Kajita, Y.; Yamaguchi, S.; Arii, H.; Ozawa, T.; Jitsukawa, K.; Tosha, T.; Hirota, S.; Kitagawa, T.; Masuda, H. Formation of a Bridged butterfly-type μ-η^2:η^2-peroxo dicopper core structure with a carboxylate group. *J. Am. Chem. Soc.* **2008**, *130*, 16444.
(31) Gagne, R. R.; Koval, C. A.; Lisensky, G. C. Ferrocene as an internal standard for electrochemical measurements. *Inorg. Chem.* **1980**, *19*, 2854.
(32) Walton, P. H.; Davies, G. J. On the catalytic mechanisms of lytic polysaccharide monooxygenases. *Curr. Opin. Chem. Biol.* **2016**, *31*, 195.
(33) *CrysAlis PRO*; Agilent Technologies Ltd: Yarnton, Oxfordshire, England, 2013.
(34) Clark, R. C.; Reid, J. S. The analytical calculation of absorption in multifaceted crystals. *Acta Crystallogr., Sect. A: Found. Crystallogr.* **1995**, *51*, 887.
(35) (a) Sheldrick, G. M. SHELXT - Integrated space-group and crystal-structure determination. *Acta Crystallogr., Sect. A: Found. Adv.* **2015**, *71*, 3. (b) Sheldrick, G. M. Crystal structure refinement with SHELXL. *Acta Crystallogr., Sect. C: Struct. Chem.* **2015**, *71*, 3−8.
(36) Farrugia, L. J. WinGX suite for small-molecule single-crystal crystallography. *J. Appl. Crystallogr.* **1999**, *32*, 837.
(37) Frisch, M. J.; Trucks, G. W.; Schlegel, H. B.; Scuseria, G. E.; Robb, M. A.; Cheeseman, J. R.; Scalmani, G.; Barone, V.; Petersson, G. A.; Nakatsuji, H.; Li, X.; Caricato, M.; Marenich, A.; Bloino, J.; Janesko, B. G.; Gomperts, R.; Mennucci, B.; Hratchian, H. P.; Ortiz, J. V.; Izmaylov, A. F.; Sonnenberg, J. L.; Williams-Young, D.; Ding, F.; Lipparini, F.; Egidi, F.; Goings, J.; Peng, B.; Petrone, A.; Henderson, T.; Ranasinghe, D.; Zakrzewski, V. G.; Gao, J.; Rega, N.; Zheng, G.; Liang, W.; Hada, M.; Ehara, M.; Toyota, K.; Fukuda, R.; Hasegawa, J.; Ishida, M.; Nakajima, T.; Honda, Y.; Kitao, O.; Nakai, H.; Vreven, T.; Throssell, K.; Montgomery, J. A., Jr.; Peralta, J. E.; Ogliaro, F.; Bearpark, M.; Heyd, J. J.; Brothers, E.; Kudin, K. N.; Staroverov, V. N.; Keith, T.; Kobayashi, R.; Normand, J.; Raghavachari, K.; Rendell, A.; Burant, J. C.; Iyengar, S. S.; Tomasi, J.; Cossi, M.; Millam, J. M.; Klene, M.; Adamo, C.; Cammi, R.; Ochterski, J. W.; Martin, R. L.; Morokuma, K.; Farkas, O.; Foresman, J. B.; Fox, D. J. *Gaussian 09*, revision A.02; Gaussian, Inc.: Wallingford CT, 2016.
(38) (a) Becke, A. D. Density-functional thermochemistry. III. The role of exact exchange. *J. Chem. Phys.* **1993**, *98*, 5648. (b) Lee, C.; Yang, W.; Parr, R. G. Development of the Colle-Salvetti correlation-energy formula into a functional of the electron density. *Phys. Rev. B* **1988**, *37*, 785.
(39) Hay, P. J.; Wadt, W. R. Ab initio effective core potentials for molecular calculations. Potentials for K to Au including the outermost core orbitals. *J. Chem. Phys.* **1985**, *82*, 299.
(40) (a) Hariharan, P. C.; Pople, J. A. The influence of polarization functions on molecular orbital hydrogenation energies. *Theor. Chim. Acta.* **1973**, *28*, 213. (b) Francl, M. M.; Petro, W. J.; Hehre, W. J.; Binkley, J. S.; Gordon, M. S.; DeFrees, D. J.; Pople, J. A. Self-consistent molecular orbital methods. XXIII. A polarization-type basis set for second-row elements. *J. Chem. Phys.* **1982**, *77*, 3654.
(41) (a) Tomasi, J.; Persico, M. Molecular Interactions in Solution: An Overview of Methods Based on Continuous Distributions of the Solvent. *Chem. Rev.* **1994**, *94*, 2027. (b) Amovilli, C.; Barone, V.; Cammi, R.; Cances, E.; Cossi, M.; Mennucci, B.; Pomelli, C. S.; Tomasi, J. Recent advances in the description of solvent effects with the polarizable continuum model. *Adv. Quantum Chem.* **1998**, *32*, 227.
(42) (a) Trasatti, S. The absolute electrode potential: an explanatory note (Recommendations 1986). *Pure Appl. Chem.* **1986**, *58*, 955. (b) Persson, I. Solvation and complex formation in strongly solvating solvents. *Pure Appl. Chem.* **1986**, *58*, 1153.
(43) Llunell, M.; Casanova, D.; Cirera, J.; Alemany, P.; Alvarez, S. *SHAPE*, version 2.0; Barcelona, 2010.
(44) McCreery, R. *Raman Spectroscopy for Chemical Analysis*; John Wiley & sons, Inc.: New York, 2000; Chapter 10.
(45) https://www.effemm2.de/spectragryph/.

DOI: 10.1021/acsomega.9b00785
ACS Omega 2019, 4, 10729−10740